Acta Cryst. (1983). A**39**, 792–800

Geometrical Aspects of Thermal Diffuse Scattering and the Associated γ-ray and X-ray Kikuchi Effects Near a Bragg Reflexion

BY S. W. WILKINS AND L. T. CHADDERTON

CSIRO, Division of Chemical Physics, PO Box 160, *Clayton, Victoria, Australia* 3168

AND T. F. SMITH

Physics Department, Monash University, Clayton, Victoria, Australia 3168

(*Received* 4 *November* 1982; *accepted* 1 *June* 1983)

Abstract

Sharp dips which are observed in inelastic thermal diffuse γ-ray scattering intensities, and which move rigidly when the crystal is rotated, are attributed to a γ-ray Kikuchi effect. Some geometrical aspects of the effect are explored using the $(\Delta 2\theta, \Delta\omega)$ approach recently developed by Mathieson [*Acta Cryst.* (1982), A**38**, 378–387] for disecting a Bragg reflexion. In particular, it is shown that observation of the effect should *not* be very sensitive to angular divergence of the incident γ-ray beam, but should depend on the effective source size, the angular resolution of the detector and on basic crystal properties such as size, absorption coefficient and mosaicity. Some useful general results for coordinate transformations between reciprocal space and $(\Delta 2\theta, \Delta\omega)$ space are also presented.

1. Introduction

γ-ray diffraction may be used to separate elastic and inelastic scattering under Bragg peaks with an energy resolution of the order of 10^{-8} eV, by means of nuclear resonance absorption of the γ-rays emitted recoilessly from a Mössbauer source. This technique has been used to study thermal diffuse scattering (TDS) by crystals, *e.g.* O'Connor & Butt (1963), Butt & O'Connor (1967), Butt & Solt (1971), Zasimov, Lobanov, Rüdiger & Kuz'min (1976) and Albanese, Chezzi, Merlin & Pace (1972), and in some cases where the system is known to undergo a phase transition, *e.g.* Lin, Spalt & Batterman (1976), Jex, Müllner, Knoth & Loidl (1980) and Ti, Finlayson, Smith, Cashion & Clark (1983). In many of these experiments a sharp (relative to the angular divergence of the incident beam) dip in the TDS has been observed, *e.g.* O'Connor & Butt (1963) for the 200 reflexion of LiF, Zasimov *et al.* (1976) for the 002 reflexion of pyrolytic graphite (*cf.* Müllner, Maetz & Jex, 1979), Kashiwase, Kainuma & Minoura (1982*a*) for the 200, 400 and 600 reflexions from KCl, and Ti *et al.* (1983) for the 440 reflexion from V_3Si. It is possible that anomalies in TDS could occur as a result of the intrinsic physical properties for certain materials (such as V_3Si), where there are corresponding anomalies in the elastic behaviour which are often accompanied by a phase transition. However, this cannot be the case for systems such as KCl, where there is no anomalous elastic behaviour.

Various explanations for the effect have been suggested, in particular:

(i) O'Connor & Butt (1963) attributed the dips to extinction effects;

(ii) Zasimov *et al.* (1976) offered an explanation involving mosaic blocks and a minimum wavevector magnitude, q_{min}, such that phonons with $q < q_{min}$ are forbidden, q_{min} being characteristic of the mosaic block sizes in the crystal; and

(iii) Müllner *et al.* (1979) propose that the dips be attributed to incorrect values of the absorber efficiency.

More recently, Kashiwase, Kainuma & Minoura (1982*a*) have carried out a detailed investigation of the effect for KCl using a position-sensitive proportional detector (PSPD). These authors concluded that the dip in their TDS profiles arose from secondary elastic scattering of the TDS away from the diffracted beam direction, *i.e.* a form of extinction of the TDS. Although this interpretation lacks clarity concerning detail and also is confusing in some respects regarding the angular divergence of the source, we believe it to contain the essence of a correct explanation for many of the dips found in TDS data measured using the Mössbauer technique. The basic physical phenomenon is essentially the γ-ray analogue of the Kikuchi effect, which is well known in electron diffraction (Kikuchi, 1928; or, for a general discussion, see, for example, Cowley, 1975; Hirsch, Howie, Nicholson, Pashley & Whelan,

0108-7673/83/050792-09$01.50

1965). The effect has recently been observed with X-rays by Kashiwase, Kainuma & Minoura (1981, 1982*b*,*c*). A corresponding classical mechanical Kikuchi effect is also found to occur in the blocking and channelling of fast charged heavy particles (Chadderton, 1966, 1970).

The terminology adopted in the present paper is to refer to characteristic lines arising from Bragg diffraction of *inelastically scattered* γ- or X-rays as Kikuchi lines. Such lines are therefore quite distinct from those arising from purely *elastic scattering* out of, say, a divergent incident beam. These are called Kossel lines (Kossel, 1935; Kossel & Voges, 1935; Lonsdale, 1947), in keeping with current terminology in electron diffraction (see *e.g.* Cowley, 1975), though if no clear distinction is made, they are often termed *K* lines (*e.g.* Cowley, 1975).

The salient features of Kashiwase *et al.*'s results for KCl are that:

(i) the dips in the TDS move such that $\Delta 2\theta = \Delta\omega$, where $\Delta 2\theta$ denotes the angular setting of the detector pixel or slit away from the Bragg condition, and $\Delta\omega$ is the offset of the crystal rocking angle away from the Bragg condition, all being taken in the plane of diffraction (see Fig. 1);

(ii) the dips in the TDS are quite sharp (typically with FWHM $\sim 0{\cdot}3°$ in $\Delta 2\theta$) and quite deep, often down to near-zero intensity;

(iii) the TDS profiles in some cases tend to be markedly asymmetric about the dip, especially when $\Delta\omega$ is large.

In order to help establish rules for ascertaining the origin of dips in inelastic scattering, particularly when these may reflect intrinsic solid-state properties of the sample such as soft modes near a phase transition, we first explore briefly some of the geometrical aspects of TDS and the γ-ray Kikuchi effect (*cf.* Kainuma, 1961).

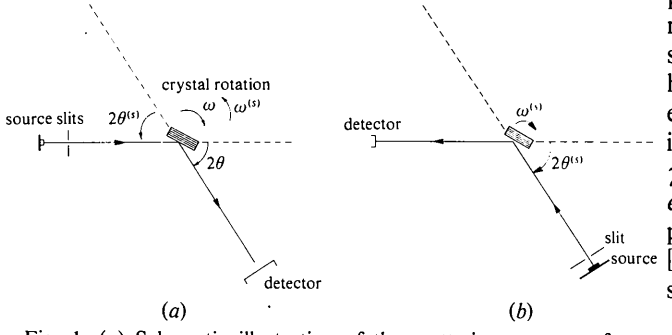

Fig. 1. (*a*) Schematic illustration of the scattering geometry for resonant Mössbauer scattering in the plane of diffraction for the case of the rotating-crystal ($\Delta\omega$) – rotating-detector ($\Delta 2\theta$) configuration. (*b*) Corresponding illustration for the rotating-crystal ($\Delta\omega^{(s)}$) – rotating source ($\Delta 2\theta^{(s)}$) configuration.

2. Characteristics of the resonant γ-ray diffractometer and of the scattering geometry

The resonant γ-ray diffractometer arrangement differs from that of a conventional X-ray diffractometer in that it has extremely well-defined wavelength with $\Delta\lambda/\lambda \sim 10^{-12}$, and permits extremely sharp discrimination between elastically and inelastically scattered photons, to the extent that inelastic scattering events involving energy transfer of the order of 10^{-8} eV may be discriminated.

However, because γ-ray sources are very weak by X-ray standards, the sources tend to be large in area. Typical γ-ray count rates on the Bragg condition are 100's of counts min^{-1}. The angular collimation of the incident beam is accordingly poor, and large sample crystals are used.

Although the γ-ray diffractometer is very sensitive for detecting the inelastic scattering of γ-rays, it should be appreciated that, for the purposes of exploring the scattering geometry of the instrument, the magnitude of the momentum of the one-phonon scattered γ-rays remains constant to ~ 1 part in 10^6. Thus the usual procedures for depicting *elastic* X-ray scattering may be employed, the Ewald-sphere construction in this case denoting the conservation-of-energy condition (see Fig. 2), at least to within a small number of phonon energies. Throughout the present work, quantities in reciprocal space are calculated assuming $\lambda = 1$ so that, for example, $\mathbf{k}_0^*$ and $\mathbf{k}_S^*$ in Fig. 2 are unit vectors. Vectors in reciprocal space are distinguished with an asterisk.

3. Reciprocal space and its relation to ($\Delta 2\theta$,$\Delta\omega$) space

In conventional X-ray diffraction the diffractometer typically has two variable angular settings (see Fig. 1*a*): $\Delta\omega$, the rocking angle of the crystal, and $\Delta 2\theta$, the angular setting of the detector pixel. Both lie in the plane of diffraction and are measured relative to the reference direction of the incident beam. It is these very same operational parameters of a diffractometer which have recently been used by Mathieson (1982, 1983*a*) in exploring the nature of the X-ray intensity distribution in the neighbourhood of a Bragg reflexion. In the γ-ray case, the detector may often be immovable (see *e.g.* Ti, Clark & Cashion, 1982) so that the operational parameters are in practice the crystal setting angle [$\Delta\omega^{(s)}$] and the source setting [$\Delta 2\theta^{(s)}$], which are simply related to $\Delta 2\theta$ and $\Delta\omega$ (see Appendix *A*).

A reciprocal-space diagram showing the exact Bragg condition in the plane of diffraction, using the Ewald construction, is given in Fig. 2(*a*). This shows the incident- and diffracted-beam unit vectors $\mathbf{k}_0^*$ and $\mathbf{k}_s^*$, respectively, together with the reciprocal-lattice vector

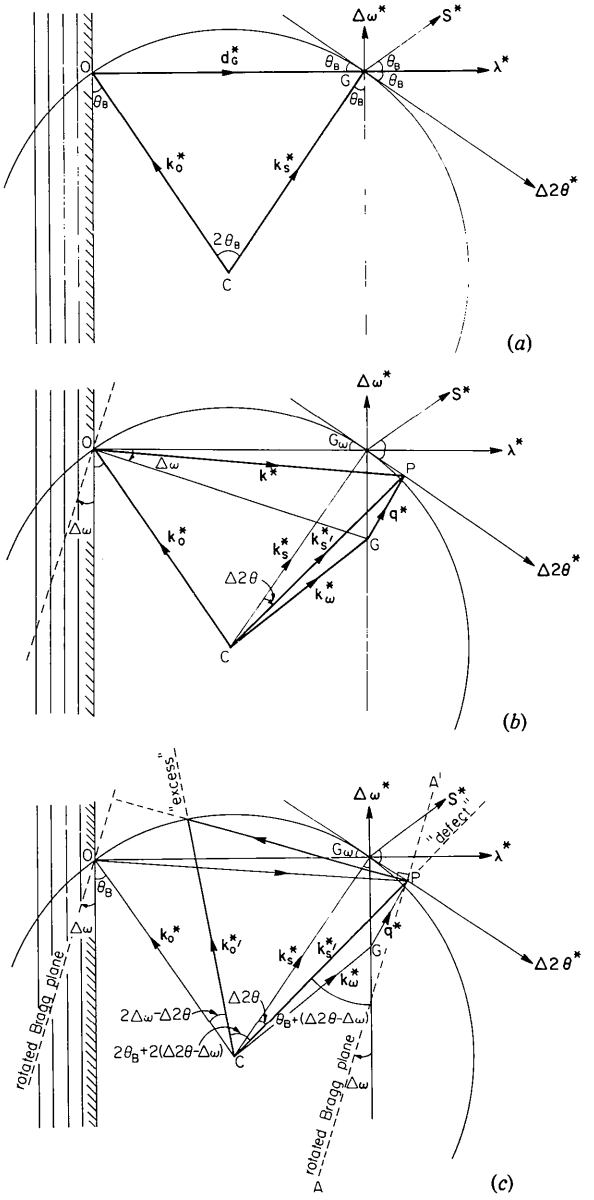

Fig. 2. (*a*) Ewald construction at the *exact* Bragg condition for scattering from the r.l.p. G (with r.l.v. $\mathbf{d}_G^*$) involving unit scattering vectors $\mathbf{k}_0^*$ (incident beam) and $\mathbf{k}_s^*$ (scattered beam). With variation of the various experimental scattering parameters the sampling point in reciprocal space moves as follows: (i) along $\boldsymbol{\lambda}^*$ for variation of λ; (ii) along $\boldsymbol{\Delta\omega}^*$ for rotation of the crystal about the normal to the plane of diffraction; (iii) along $\boldsymbol{\Delta 2\theta}^*$ for rotation of the detector; and (iv) along $\mathbf{S}^*(\perp\mathbf{k}_0^*)$ for variation in the angle of incidence (*i.e.* angular divergence of the source). (*b*) Ewald construction for scattering when both the crystal ($\Delta\omega$) and detector are offset from the exact Bragg condition. The r.l.p. G has moved from G_ω, while the detector is at P, so the new scattered-wave vector is $\mathbf{k}_{s'}^*$ and the reciprocal-space vector (phonon wave vector) connecting P and G is $\mathbf{q}^*$. (*c*) The origins of the Kikuchi effect which arises when the diffusely scattered beam $\mathbf{k}_{s'}^*$ is at the correct angle (*i.e.* $\Delta 2\theta = \Delta\omega$) for Bragg scattering from the rotated Bragg planes (dashed line AA' through P), *i.e.* $\mathbf{k}_{s'}^*$ becomes the incident beam (giving a 'defect line') and $\mathbf{k}_0$ the new diffracted beam (giving an 'excess line') for an Ewald construction taken relative to P as origin.

(r.l.v.) $\mathbf{d}_G^*$ to the reciprocal-lattice point (r.l.p.) G, and also the directions at G of the principal instrumental and sample factors in reciprocal space. These are:

(i) the crystal rocking-angle direction $\boldsymbol{\Delta\omega}^*$, which is perpendicular to $\mathbf{d}_G^*$, and is defined positive in the sense that clockwise rotation of the crystal looking down on the plane of diffraction leads to a sampling of reciprocal space in the positive v direction (see Figs. 2*a* and 3);

(ii) the wavelength direction $\boldsymbol{\lambda}^*$, which is parallel to $\mathbf{d}_G^*$ through G;

(iii) the direction $\boldsymbol{\Delta 2\theta}^*$, which is tangential to the Ewald sphere at G and at an angle of $-\theta_B$ to $\boldsymbol{\lambda}^*$;

(iv) the source-distribution direction $\mathbf{S}^*$, which is perpendicular to $\mathbf{k}_0^*$ through G.

Thus, for example, the presence of a mosaic distribution of crystallites leads to a smearing out of the reciprocal lattice along $\boldsymbol{\Delta\omega}^*$, while angular divergence in the incident beam leads to a smearing out of the sampling of reciprocal space along $\mathbf{S}^*$. Finite resolution of the detector (*e.g.* pixel size in a PSPD) leads to smearing out of the sampling of reciprocal space along $\boldsymbol{\Delta 2\theta}^*$. When two or more factors are simultaneously present, the combined effect is typically treated as a convolution, and a 'resolution ellipsoid' in reciprocal space results (Cooper & Nathans, 1967; and also § 5). The effect on reciprocal-space sampling of, for example, a movement of the detector away from the Bragg condition by a small offset $\Delta 2\theta$ (Fig. 2*b*) is to displace the scattered-beam direction along $\boldsymbol{\Delta 2\theta}^*$ from G to P (under the tangential approximation). The vector for sampling in reciprocal space is then given by OP. On the other hand, if the crystal is rocked by a small angle $\Delta\omega$, then the

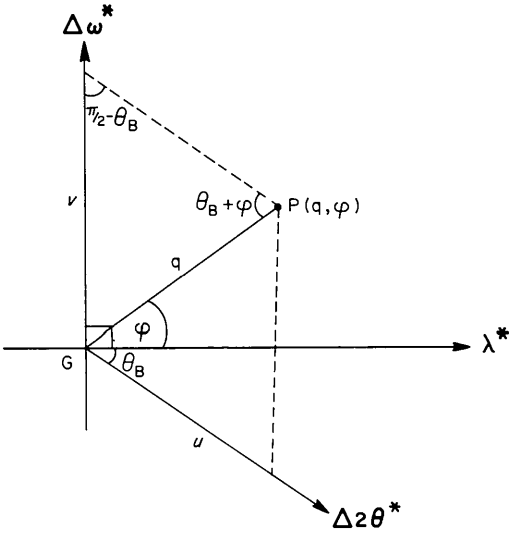

Fig. 3. Diagram of reciprocal space about G showing the relationship between the oblique coordinate system with $\boldsymbol{\Delta 2\theta}^*$ and $\boldsymbol{\Delta\omega}^*$ as axes [coordinates (u,v)] and the rectangular system taking $\boldsymbol{\lambda}^*$ and $\boldsymbol{\Delta\omega}^*$ as axes [*i.e.* coordinates (q_λ, q_ω)].

reciprocal-lattice point moves in the $-\Delta\boldsymbol{\omega}^*$ direction from G_ω to G, and the new origin of coordinates is taken to be at G. Thus, if the detector remains fixed at $\Delta 2\theta = 0$, then the diffracted beam is sampled at the point G_ω relative to G (Fig. 2*b*), and this is in the positive $\Delta\boldsymbol{\omega}^*$ direction. More generally, the two variations may be considered to occur simultaneously (Fig. 2*b*) so that the new diffraction setting of the instrument is $(\Delta 2\theta,\Delta\omega)$, corresponding to a general point P in reciprocal space, expressed here in either polar coordinates (q,φ) or rectangular coordinates (q_λ,q_ω) about G.

The oblique coordinates, (u,v), in reciprocal space of the point $(\Delta 2\theta,\Delta\omega)$ are (see Fig. 3)

$$u = \Delta 2\theta;\ v = (2\sin\theta_B)\,\Delta\omega, \tag{1}$$

which, in turn, give for the polar coordinates (q,φ) and rectangular coordinated (q_λ,q_ω) of P the expressions

$$\Delta 2\theta = \frac{\cos\varphi}{\cos\theta_B}\,q;\quad \Delta\omega = \frac{\sin(\theta_B+\varphi)}{\sin 2\theta_B}\,q$$

and

$$\begin{bmatrix}\Delta 2\theta\\ \Delta\omega\end{bmatrix} = \frac{1}{\sin 2\theta_B}\begin{bmatrix}2\sin\theta_B & 0\\ \sin\theta_B & \cos\theta_B\end{bmatrix}\begin{bmatrix}q_\lambda\\ q_\omega\end{bmatrix}. \tag{2}$$

Thus the relationship between the reciprocal space, (q_λ,q_ω), and $(\Delta 2\theta,\Delta\omega)$-space coordinate systems is that of a *homogeneous affine transformation*. Parallel straight lines in one space map into parallel straight lines in the other space, ellipses map into ellipses, and equally spaced points on one straight line map into equally spaced points on another straight line. The origin is an invariant point.

It is useful to consider the relationship between $(\Delta 2\theta,\Delta\omega)$ space and reciprocal space, for the following special cases.

3.1. *Straight line at angle φ_0 to $\boldsymbol{\lambda}^*$*

A straight line through G at an angle φ_0 to $\boldsymbol{\lambda}^*$ has the equation

$$\Delta\omega = \tfrac{1}{2}[1+\cot\theta_B\tan\varphi_0]\,\Delta 2\theta \equiv \frac{1}{\sigma}\,\Delta 2\theta; \tag{3}$$

therefore, in order to scan along a line at this angle to $\boldsymbol{\lambda}^*$ in reciprocal space and in the plane of diffraction, a scan ratio of $\sigma \equiv \Delta 2\theta/\Delta\omega$ is required. For example, a scan parallel to $\mathbf{S}^*$ ($\varphi_0 = \theta_B$) requires $\sigma = 1$, which corresponds to an ω/θ scan where detector and crystal are rotated together with equal incremental steps.

3.2. *Circle centred at G*

A circle of radius q centred at G in reciprocal space has the equation in $(\Delta 2\theta,\Delta\omega)$ space:

$$(\Delta 2\theta)^2 - 4\sin^2\theta_B\,\Delta\omega\Delta 2\theta + 4\sin^2\theta_B\,\Delta\omega^2 = q^2, \tag{4}$$

which describes an ellipse whose major axis lies at an angle ψ to the $\Delta 2\theta$ axis, where

$$\tan 2\psi = -4\sin^2\theta_B/[1-4\sin^2\theta_B]. \tag{5}$$

4. Thermal diffuse scattering and the γ-ray Kikuchi effect

The Kikuchi effect essentially arises when inelastic diffuse radiation generated *within* the crystal is incident on crystal planes at the proper angle to undergo a Bragg reflexion (see *e.g.* Cowley, 1975). In the case of γ-rays, the principal source of diffuse scattering for a crystal set near to a Bragg reflexion is from TDS about that Bragg reflexion. Geometrically, this occurs when the rotated Bragg planes AA' (Fig. 2*c*) are at the correct angle for Bragg diffraction of the diffusely scattered beam $\mathbf{k}_s^*$, *i.e.* so that the angle CPA is equal to the Bragg angle, θ_B. This condition requires that

$$\Delta 2\theta + \theta_B = \Delta\omega + \theta_B, \tag{6}$$

which in turn leads to the condition for the γ-ray Kikuchi effect:

$$\Delta 2\theta = \Delta\omega, \tag{7}$$

indicating that the Kikuchi point, P, moves rigidly with the crystal and gives a Kikuchi locus in $(\Delta 2\theta,\Delta\omega)$ space lying along the direction of an ω/θ scan in the plane of diffraction. More generally, the defect Kikuchi line for given $\Delta\omega$ extends perpendicular to the plane of diffraction through $(\Delta 2\theta,\Delta\omega)$, see *e.g.* Hirsch *et al.* (1965). Concomitant with the depletion in intensity of the diffuse radiation at $\Delta 2\theta$, there is of course an excess intensity Kikuchi line near the incident beam and at angular position $\Delta\omega = \Delta 2\theta$ away from O (see Fig. 2*c*).

4.1. *Isotropic thermal diffuse scattering*

To illustrate geometrical aspects of the γ-ray Kikuchi effect, we first consider the simple case of an isotropic distribution of TDS intensity about G (see *e.g.* Willis & Pryor, 1975), namely

$$I_{\mathrm{TDS}}(q) = c/q^2, \tag{8}$$

where $\mathbf{q}$ is the vector displacement in reciprocal space of the observation point, P, away from the rotated reciprocal-lattice point, G (see Fig. 2*b*), and is equal to the phonon wave vector for a one-phonon scattering process from G to P. For small q, the form (8) arises from the long-wavelength acoustic phonons. More generally, however, it may also contain an angular factor consistent with the point-group symmetry of the r.l.p., which is present, in general, even for an elastically isotropic crystal (see *e.g.* Walker & Chipman, 1970).

Substituting (4) for q^2 in (8), we transform the reciprocal-space TDS distribution into $(\Delta 2\theta,\Delta\omega)$ space to obtain

$$I_{\mathrm{TDS}} = c[(\Delta 2\theta)^2 - 4\sin^2\theta_B\,\Delta\omega\,\Delta 2\theta + 4\sin^2\theta_B\,\Delta\omega^2]^{-1}. \quad (9)$$

A Mathieson (contour) plot of this function in $(\Delta 2\theta,\Delta\omega)$ space (Mathieson, 1982) is given in Fig. 4 for $\theta_B = 25°$, which approximates the 600 reflexion of KCl with 14·4 keV γ-rays. Included on the plot are lines through G corresponding to: (i) the locus of the Kikuchi effect (K); (ii) the major axis of the TDS ellipse (E); (iii) the maximum of the TDS for a $\Delta 2\theta$ scan (*i.e.* with fixed $\Delta\omega$)

$$\Delta 2\theta^{\max} = (2\sin^2\theta_B)\,\Delta\omega; \quad (10)$$

and (iv) the maximum of the TDS for a $\Delta\omega$ scan (*i.e.* with fixed $\Delta 2\theta$)

$$\Delta\omega^{\max} = \tfrac{1}{2}\Delta 2\theta. \quad (11)$$

Thus, for example, (10) describes the linear locus, as a function of $\Delta\omega$, of the maxima of the TDS in the $\Delta 2\theta$ scans of the type presented by Kashiwase, Kainuma & Minoura (1982*a*), which would be expected if the TDS were isotropic. Positions of the various important features in the TDS profile, such as the Kikuchi minimum and the TDS maximum as a function of $\Delta\omega$ using $\Delta 2\theta$ scans [*i.e.* profiles such as those obtained by Kashiwase, Kainuma & Minoura (1982*a*) with a stationary PSPD] are readily predicted using Fig. 4. Only when the crystal and detector are exactly set for the Bragg condition (*i.e.* $\Delta 2\theta = \Delta\omega = 0$) do all features coincide. This provides a means of orienting crystals using TDS and quite analogous to the well-known method in electron diffraction and microscopy using the Kikuchi lines and bands (see *e.g.* Hirsch *et al.*, 1965). In practice, the zero point for the ω scale on a diffractometer is ill defined, and consequently the value of $\Delta\omega$ will be affected. Accordingly, values of $\Delta\omega$ quoted by Kashiwase *et al.* (1982*a*) should not be regarded as absolute, but rather as indicating that the condition $\Delta\omega = 0$ may be established empirically using the Kikuchi effect and other TDS features. For example, $\Delta\omega$ in their Fig. 6 would seem to be very nearly zero, rather than the $-9'$ quoted.

The effect on the TDS contours of changing θ_B is illustrated in Fig. 5. For small θ_B the TDS ellipse is elongated along the $\Delta\omega$ axis, while for increasing θ_B (up to $\pi/2$), the TDS ellipse rotates until the major axis lies along the line $\Delta\omega = \frac{1}{2}\Delta 2\theta$ corresponding to the λ direction.

4.2. *Anisotropic thermal diffuse scattering*

Although perhaps not immediately obvious from Fig. 4, both $\Delta 2\theta$ and $\Delta\omega$ scans for spherically symmetrical TDS distributions are symmetrical about their respective maxima, as can be seen by examination of (4) and (8). However, the introduction of an angular factor in (8) leads in general to asymmetric TDS profiles. If we assume one-phonon scattering, (8) becomes (see *e.g.* Willis & Pryor, 1975)

$$I_{\mathrm{TDS}}(q) = \frac{c}{q^2}[1 + A(\varphi)], \quad (12)$$

where q^2 is given by (4) and $A(\varphi)$ is an angular factor which must satisfy the appropriate point-group symmetry of a r.l.p., taking into account the orientation of the plane of diffraction in reciprocal space, the lowest possible symmetry being that of a centre of inversion. In order to illustrate the effect of anisotropy of TDS in reciprocal space on Mathieson plots, we have con-

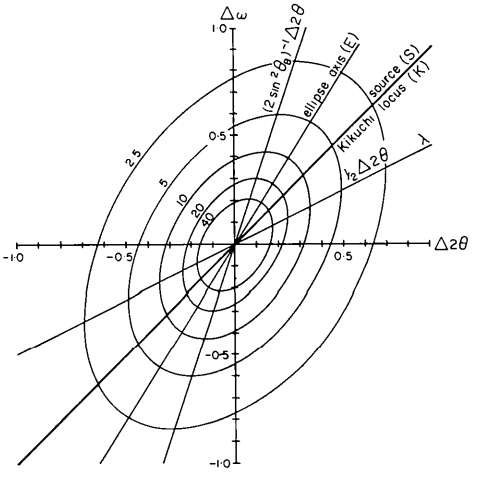

Fig. 4. Mathieson plot showing TDS contours in $(\Delta 2\theta,\Delta\omega)$ space corresponding to isotropic TDS contours in reciprocal space. Also shown are : (i) the ellipse major axis (along E); (ii) the locus of TDS maxima for $\Delta 2\theta$ scans $1/(2\sin^2\theta_B)$; and (iii) TDS maxima for $\Delta\omega$ scans ($\frac{1}{2}\Delta 2\theta$).

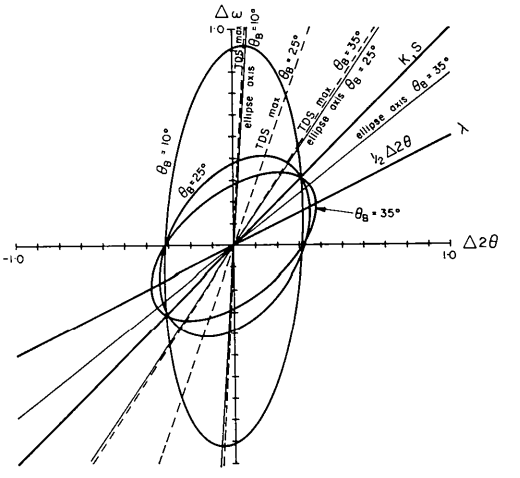

Fig. 5. Mathieson plot showing TDS contours in $(\Delta 2\theta,\Delta\omega)$ space corresponding to isotropic TDS in reciprocal space for various values of θ_B with: (i) ellipse major axes (solid lines); and (ii) locii of TDS maxima in $\Delta 2\theta$ scans (dashed lines).

sidered the special case of a cubic crystal, for which a simple analytical expression for $A(\varphi)$ is available (Waller, 1925; Walker & Chipman, 1970). Values of elastic constants appropriate for KCl at room temperature (Enck, 1960) have been used and the results for a 600-type reflexion (Fig. 6) and a 660 reflexion (Fig. 7) have been plotted (see also Lonsdale, 1942). In the case of 600 the elastic anisotropy has displaced the TDS maximum so that it lies close to the $\Delta\omega$ axis. Thus both $\Delta 2\theta$ or $\Delta\omega$ profiles of the TDS are very nearly symmetrical. Modification to the shape of the intensity contours for the 660 reflexion with the introduction of anisotropic TDS is, however, more complex than for the 600 reflexion, and this further complicates the Mathieson plots. As can be seen from Fig. 7, the locus of the TDS maximum for the anisotropic case moves only slightly towards higher $\Delta 2\theta$, relative to the case for the isotropic crystal, but the $\Delta 2\theta$ or $\Delta\omega$ profiles of the TDS are now highly asymmetrical in general. Nevertheless, it should be noted that TDS profiles through the origin are always symmetrical (the origin being a centre of inversion), and that the asymmetry in the profiles increases with increasing distance of the scan away from the origin.

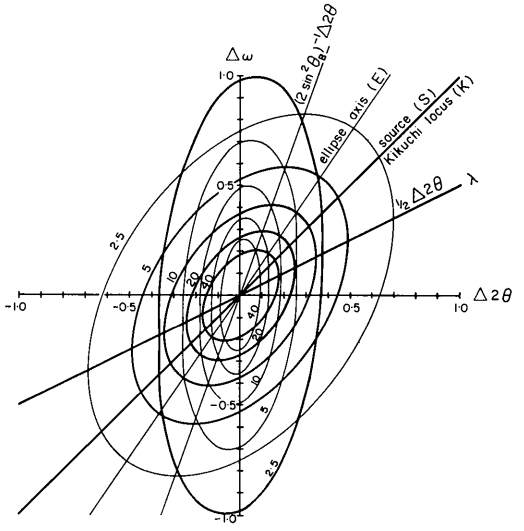

Fig. 6. TDS contours in $(\Delta 2\theta,\Delta\omega)$ space corresponding to the $(h,k,0)$ plane of reciprocal space for the isotropic TDS case (thin contours) and an elastically anisotropic cubic crystal (thick contours) ($\theta_B = 25°$ and a 600 reflexion).

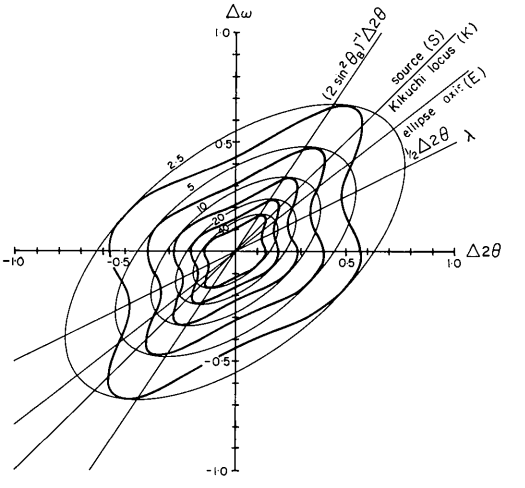

Fig. 7. Mathieson plot showing TDS contours in $(\Delta 2\theta,\Delta\omega)$ space for isotropic TDS in reciprocal space and an elastically anisotropic cubic crystal ($\theta_B = 35°$ and 660 reflexion).

4.3. *Other sources of asymmetry in scattering profiles*

In addition to asymmetry arising from the intrinsic character of the TDS contours about a r.l.p., the following physical factors could also lead to asymmetry in measured TDS profiles:

(i) a non-centrosymmetric distribution of scattering due to non-uniformity in the angular and size distribution of mosaic blocks;

(ii) anomalous absorption – especially when the sample is nearly perfect (see Takagi, 1958; Olekhnovich & Olekhnovich, 1981);

(iii) intrinsic resolution factors of the instrument (see § 5).

5. Resolution and crystal factors

No measuring instrument is perfect. Sampling of reciprocal space by a diffractometer is always necessarily smeared out to a greater or lesser extent by instrumental factors such as source size (s), angular divergence of the incident beam (d), wavelength spread (L), and angular resolution of detector (D). In addition, such properties of the crystal as size (c) and mosaic distribution (M) inevitably lead to a further smearing out in the sampling of reciprocal space. The vector nature of the various resolutional and crystal factors is displayed in Fig. 8. In practice, all are present simultaneously (with the exception in the γ-ray case of the $\Delta\lambda$ spread) and are typically assumed to combine convolutionally leading, for say Gaussian distributions, to a resolution ellipsoid in either reciprocal or $(\Delta 2\theta,\Delta\omega)$ space (Cooper & Nathans, 1967). An important feature which is clear from Fig. 8 is that the effects of angular divergence of the source (*i.e.* S_{dc} and S_{ds}) lie along the $\Delta 2\theta = \Delta\omega$ line, or Kikuchi-line locus in $(\Delta 2\theta,\Delta\omega)$ space. Thus a high degree of incident-beam collimation is certainly *not* crucial for observation of the Kikuchi effect (*cf.* Kashiwase *et al.*, 1982*a*,*b*,*c*). Kikuchi effects which are much narrower than the angular divergence of the incident beam are to be expected (see *e.g.* Ti *et al.*, 1983), a fact well known in electron diffraction, where Kikuchi lines involving

inelastic scattering of electrons can also be observed with convergent beams (Carpenter & Spence, 1982), as well as Kossel lines which arise from *elastic* scattering of the electrons. Such Kikuchi lines are more readily observed by having an extremely small source size.

6. Conditions favouring a strongly observable γ-ray Kikuchi effect

As pointed out in the previous section, angular divergence of the incident beam is not a crucial factor in the observability of Kikuchi lines. On the other hand, from the physical origins of the effect and the associated geometrical conditions, the following factors would appear to be important in determining the magnitude and sharpness of the Kikuchi effect.

(i) The angular resolution of the detector in $\Delta 2\theta$ must be better than the angular width of the Kikuchi line (see Fig. 8).

(ii) The mosaicity of the specimen will largely determine both the natural width and visibility of the Kikuchi line (Lonsdale, 1947; Bushuev, Laushkin, Kuz'min & Lobanov, 1981); the more perfect the crystal, the narrower the Kikuchi line. On the other hand, viewed from the other extreme of the 'ideally imperfect' crystal, where the Kikuchi effect would be absent, one would first expect the visibility of the Kikuchi effect to increase with the increase in the degree of perfection due to the increase in reflectivity, but eventually to decrease towards the perfect-crystal limit due to instrumental broadening of the line and decrease in integrated reflectivity.

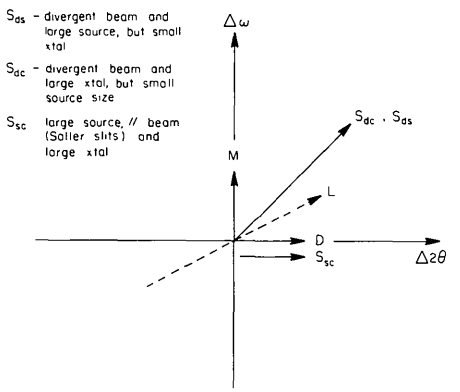

Fig. 8. Simple illustration of resolution factors in $(\Delta 2\theta,\Delta\omega)$ space for the resonant γ-ray diffractometer, with smearing out of sampling volume in reciprocal arising from: (i) D – detector resolution (along $\Delta 2\theta$ axis); (ii) L – finite spread in λ (not significant for resonant γ-ray experiment and so shown only as a broken vector directed along $\Delta\omega = \frac{1}{2}\Delta 2\theta$); (iii) M – effect of mosaicity of the crystal (along $\Delta\omega$ axis); (iv) S_{ds} – effect of the combination of a divergent incident beam and a large source but a small crystal (along $\Delta\omega = \Delta 2\theta$); (v) S_{dc} – effect of the combination of a divergent beam and large crystal but a small source size (along $\Delta\omega = \Delta 2\theta$); (vi) S_{sc} – effect of the combination of a large source size and large crystal but a parallel beam (along $\Delta 2\theta$ axis).

(iii) The extinction length, t_e (being that distance over which the beam is attenuated by e^{-1} due to diffraction for the given Bragg reflexion), should be small relative to the absorption length, t_a. Thus, the crystal should tend towards the highly perfect limit and the structure factor should be reasonably strong.

(iv) The crystal should be sufficiently thick in the diffracted-beam direction for there to be a significant probability for secondary Bragg scattering of the TDS. The crystal should be at least as thick as t_e, and preferably thicker.

(v) Choice of scan (coupling between $\Delta\omega$ and $\Delta 2\theta$) will influence the strength of the Kikuchi dip. The sharpest dip will occur for a scan which is normal to the locus of the Kikuchi line, *i.e.* an $(\omega/-\theta)$-space scan. Conversely, for scans *along* the locus of the Kikuchi line (*i.e.* ω/θ scans), the Kikuchi effect should be invisible.

7. Applications of the γ-ray and X-ray Kikuchi effect

Apart from its intrinsic interest, the γ-ray and X-ray Kikuchi effect will find useful applications in crystal studies. We suggest the following:

(i) orientation of crystals and determination of the $\Delta\omega = 0$ position (see *e.g.* Hirsch *et al.*, 1965);

(ii) X-ray and γ-ray energy-loss studies using the crystal as both sample and analyser (Grenville-Wells, 1951; Bushuev *et al.*, 1981). This could provide information on both the type and the location of *light* impurity atoms in a heavier material;

(iii) studies of regions where Kikuchi lines cross, whence it should prove possible to obtain phase-angle information for structural studies (see *e.g.* Hurley & Moodie, 1980; Post, 1977);

(iv) determinations of rocking-curve widths relatively free from convolution with the angular distribution of the source;

(v) combination of rocking-curve measurements (Andersen, Golovochenko & Mair, 1976) with energy studies [see (ii) above] might also provide information on both the type and location of *light* impurity atoms in a heavier matrix;

(vi) separation of intrinsic anomalies in TDS, associated with unusual physical properties of the crystal (such as soft-phonon modes) from Kikuchi and other geometrical effects.

8. Conclusion

Sharp dips which are observed in inelastic (thermal diffuse) γ-ray scattering intensities, and which move

rigidly when the sample crystal is rotated, are due to a γ-ray Kikuchi effect. An analogous neutron Kikuchi effect is also to be expected (Wilkins, 1983).

The authors are very grateful to Dr A. McL. Mathieson for numerous helpful discussions on the application of his ($\Delta 2\theta$,$\Delta\omega$) approach to the Kikuchi problem, and also to Drs J. D. Cashion, T. R. Finlayson, S. L. Mair, A. Olsen and C. J. Rossouw.

APPENDIX *A*

The rotating-source–rotating-crystal configuration

By interchanging source and detector in the geometry shown in Fig 1(*a*) and adopting the convention for directions of rotation shown in Fig. 1, the relationship between the rotating-source configuration ($\Delta 2\theta^{(s)}$,$\Delta\omega^{(s)}$) and the conventional ($\Delta 2\theta$,$\Delta\omega$) description is as follows:

$$1 = (\sigma - 1)\,(\sigma^{(s)} - 1) \qquad (A1)$$

$$\Delta 2\theta^{(s)} = \Delta 2\theta \qquad (A2)$$

$$\Delta\omega^{(s)} = (\Delta 2\theta - \Delta\omega). \qquad (A3)$$

Simple reciprocity arguments show that the scattering geometry and equivalent scattering diagrams for the rotating-source configuration (see Fig. 1) are obtained from those presented earlier (Fig. 2) by a rotation of π about the scattering vector.

APPENDIX *B*

Types of scan

In conventional diffractometry, rotations of the detector (2θ arm) and of the crystal (ω setting) are often coupled, either mechanically or by steering software.

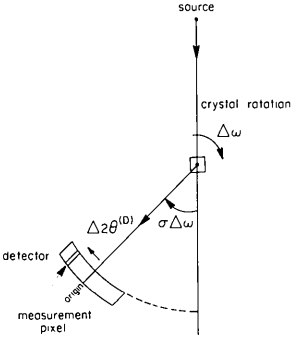

Fig. 9. Relationship between absolute angular displacement, $\Delta 2\theta$ (in laboratory frame), and relative angular displacement, $\Delta 2\theta^{(D)}$ (in detector frame), when the scan ratio (coupling between 2θ and ω axes) is σ.

The absolute angular displacement of the measurement ($\Delta 2\theta$) may be written as

$$\Delta 2\theta = \sigma\Delta\omega + \Delta 2\theta^{(D)}, \qquad (B1)$$

where the first term in ($B1$) gives the displacement due to coupled motion of the detector and crystal, with a coupling ratio of σ, and $\Delta 2\theta^{(D)}$ is the angular offset of the measurement relative to the reference position $\sigma\Delta\omega$ (see Fig. 9). In the case of a PSPD which is scanned with origin setting given by $\sigma\Delta\omega$, $\Delta 2\theta^{(D)}$ denotes the angular readings of the measurement in the frame of the moving detector relative to the origin in the detector.

If instead of working in absolute readings for $\Delta 2\theta$, one chooses to work in the offset reading, $\Delta 2\theta^{(D)}$, then

$$\begin{bmatrix}\Delta 2\theta^{(D)} \\ \Delta\omega\end{bmatrix} = \begin{bmatrix}1 & -\sigma \\ 0 & 1\end{bmatrix}\begin{bmatrix}\Delta 2\theta \\ \Delta\omega\end{bmatrix}, \qquad (B2)$$

which, on using (2), may in turn be expressed in terms of reciprocal-space coordinates. Alternatively, the reciprocal-space coordinates corresponding to a ($\Delta 2\theta^{(D)}$,$\Delta\omega$) setting are given by

$$\begin{bmatrix}q_\lambda \\ q_\omega\end{bmatrix} = \begin{bmatrix}\cos\theta_B & 0 \\ -\sin\theta_B & 2\sin\theta_B\end{bmatrix}\begin{bmatrix}1 & \sigma \\ 0 & 1\end{bmatrix}\begin{bmatrix}\Delta 2\theta^{(D)} \\ \Delta\omega\end{bmatrix}$$

$$= \begin{bmatrix}\cos\theta_B & \sigma\cos\theta_B \\ -\sin\theta_B & (2-\sigma)\sin\theta_B\end{bmatrix}\begin{bmatrix}\Delta 2\theta^{(D)} \\ \Delta\omega\end{bmatrix}, \qquad (B3)$$

so that ($\Delta 2\theta^{(D)}$,$\Delta\omega$) measurements may immediately be transferred into corresponding reciprocal-space measurements *via* ($B3$).* The transformation is clearly a homogeneous affine transformation with all the associated properties (see § 3).

References

ALBANESE, G., CHEZZI, C., MERLIN, A. & PACE, S. (1972). *Phys. Rev. B*, **5**, 1746–1757.
ANDERSEN, S. K., GOLOVCHENKO, J. A. & MAIR, G. (1976). *Phys. Rev. Lett.* **37**, 1141–1145.
BUSHUEV, V. A., LAUSHKIN, R., KUZ'MIN, R. N. & LOVANOV, N. N. (1981). *JETP Lett.* **34**, 236–239.
BUTT, N. M. & O'CONNOR, D. A. (1967). *Proc. Phys. Soc. London*, **90**, 247–252.
BUTT, N. M. & SOLT, G. (1971). *Acta Cryst.* A**27**, 238–243.
CARPENTER, R. & SPENCE, J. S. (1982). *Acta Cryst.* A**38**, 55–61.
CHADDERTON, L. T. (1966). *Phys. Lett.* **23**, 303–304.
CHADDERTON, L. T. (1970). *J. Appl. Cryst.* **3**, 429–465.
COOPER, M. J. & NATHANS, R. (1967). *Acta Cryst.* **23**, 357–367.
COWLEY, J. M. (1975). *Diffraction Physics*. Amsterdam: North-Holland.
ENCK, F. D. (1960). *Phys. Rev.* **119**, 1873–1877.
GRENVILLE-WELLS, H. J. (1951). *Nature (London)*, **168**, 290–291.
HIRSCH, P. B., HOWIE, A., NICHOLSON, R. B., PASHLEY, D. W. & WHELAN, M. J. (1965). *Electron Microscopy of Thin Crystals*. London: Butterworth.
HURLEY, A. C. & MOODIE, A. F. (1980). *Acta Cryst.* A**36**, 737–738.

* *Note added in proof: cf.* Mathieson (1983*b*).

JEX, H., MÜLLNER, M., KNOTH, R. & LOIDL, A. (1980). *Solid State Commun.* **36**, 713–716.
KAINUMA, Y. (1961). *J. Phys. Soc. Jpn*, **16**, 228–241.
KASHIWASE, Y., KAINUMA, Y. & MINOURA, M. (1981). *J. Phys. Soc. Jpn*, **50**, 2793–2794.
KASHIWASE, Y., KAINUMA, Y. & MINOURA, M. (1982*a*). *J. Phys. Soc. Jpn*, **51**, 937–941.
KASHIWASE, Y., KAINUMA, Y. & MINOURA, M. (1982*b*). *Jpn. J. Appl. Phys.* **21**, L34–36.
KASHIWASE, Y., KAINUMA, Y. & MINOURA, M. (1982*c*). *Acta Cryst.* A**38**, 390–391.
KIKUCHI, S. (1928). *Jpn. J. Phys.* **5**, 83–96.
KOSSEL, W. (1935). *Z. Phys.* **94**, S139–144.
KOSSEL, W. & VOGES, H. (1935). *Ann. Phys. (Leipzig)*, **23**, S677–704.
LIN, W., SPALT, H. & BATTERMAN, B. W. (1976). *Phys. Rev. B*, **13**, 5158–5169.
LONSDALE, K. (1942). *Proc. Phys. Soc.* **54**, 314–353.
LONSDALE, K. (1947). *Philos. Trans. R. Soc. London Ser. A*, **240**, 219–250.
MATHIESON, A. MCL. (1982). *Acta Cryst.* A**38**, 378–387.
MATHIESON, A. MCL. (1983*a*). *Acta Cryst.* A**39**, 79–83.
MATHIESON, A. MCL. (1983*b*). *J. Appl. Cryst.* **16**, 257–258.
MÜLLNER, M., MAETZ, J. & JEX, H. (1979). *Phys. Status Solidi*, **56**, 541–544.
O'CONNOR, D. A. & BUTT, N. M. (1963). *Phys. Lett.* **7**, 233–235.
OLEKHNOVICH, N. M. & OLEKHNOVICH, A. I. (1981). *Phys. Status Solidi A*, **67**, 427–433.
POST, B. (1977). *Phys. Rev. Lett.* **39**, 760–763.
TAKAGI, S. (1958). *J. Phys. Soc. Jpn*, **13**, 278–296.
TI, T. T., CLARK, P. E. & CASHION, J. D. (1982). *Nucl. Instrum. Methods*, **203**, 533–536.
TI, T. T., FINLAYSON, T. R., SMITH, T. F., CASHION, J. D. & CLARK, P. E. (1983). *Aust. J. Phys.* **36**, 185–196.
WALKER, C. B. & CHIPMAN, D. R. (1970). *Acta Cryst.* A**26**, 447–455.
WALLER, I. (1925). Dissertation, Uppsala.
WILKINS, S. W. (1983). *Phys. Rev. Lett.* **50**, 1862–1865.
WILLIS, B. T. M. & PRYOR, A. W. (1975). *Thermal Vibrations in Crystallography*, ch. 7. Cambridge Univ. Press.
ZASIMOV, V. S., LOBANOV, N. N., RÜDIGER, J. & KUZ'MIN, R. N. (1976). *Phys. Status Solidi A*, **38**, K45–47.

Acta Cryst. (1983). A**39**, 800–805

A Simple Rule for Finding and Distinguishing Triplet Phase Invariants with Values Near 0 or π with Isomorphous Replacement Data

BY JEROME KARLE

Laboratory for the Structure of Matter, Naval Research Laboratory, Washington, DC 20375, USA

(*Received* 10 *March* 1983; *accepted* 16 *May* 1983)

Abstract

On the basis of some mathematical and physical characteristics of isomorphous-replacement experiments, it has been possible to derive a simple rule called $R_{\rm iso}$ that permits the selection of those triplet phase invariants that have values close to zero or π. Test examples show that large numbers of invariants may be evaluated by means of $R_{\rm iso}$ with reliabilities that are potentially high, but depend, of course, on the reliability of the experimental data. In order to apply the rule, it is not necessary to know the chemical nature of the substituent atoms, their positions in the structure or their occupancy. The rule $R_{\rm iso}$ affords new insights into the inter-relationships among isomorphous-replacement data and an alternative selection method to the use of the conditional joint probability distribution. A formula has also been derived for estimating the value of the cosine of triplet phase invariants for the native substance, $\cos(\varphi_{\mathbf{h}P} + \varphi_{\mathbf{k}P} + \varphi_{(\mathbf{h}+\mathbf{k})P})$, in terms of measured structure-factor magnitudes and structure-factor magnitudes associated with the contribution from substituent atoms.

0108-7673/83/050800-06$01.50

Introduction

Isomorphous-replacement experiments provide information that is quite useful in selection procedures for finding large numbers of triplet phase invariants, whose values are close to zero or π, even in very complex structures. One such procedure has already been described by Hauptman (1982*a*), in which the concept of the conditional joint probability distribution has been applied to the isomorphous-replacement technique, resulting in a formula whose validity has been demonstrated in an extensive test calculation (Hauptman, Potter & Weeks, 1982). The various conceptual aspects and features of the joint probability distribution distinguish the latter approach from the one pursued in this article.

The joint probability distribution, as generally used in crystallography and from which the conditional distribution is derived, may be viewed as counting the relative number of atomic configurations (each given unit weight) associated with some infinitesimal volume in the space of the variables, say $E_1, \ldots, \varphi_1, \ldots$. In those cases where some small region of the space is